Interplay of Ionic, Hydrogen-Bonding, and Polar Interactions in Liquid Crystalline Complexes of a Pyridylpyridinium Polyamphiphile with (Azo)phenol-Functionalized Molecules

Xavier Sallenave and C. Geraldine Bazuin*

Département de chimie, Université de Montréal, C. P. 6128, succursale Centre-ville, Montréal (QC), Canada H3C 3J7

Received March 21, 2007; Revised Manuscript Received May 2, 2007

ABSTRACT: Most supramolecular side-chain polymers investigated to date are based on a single type of noncovalent link and involve systems that do not test its selectivity in the presence of other potentially interfering interactions. In this paper, we study the selectivity of hydrogen-bond complexation in the presence of both ionic moieties and highly polar groups and evaluate the effect of these potentially interacting functions on the self-assembly and thermotropic behavior of the intended side-chain liquid crystal (LC) polymer complexes. To this end, the weakly mesomorphic polyamphiphile, poly(*ω*-pyridylpyridinium dodecyl methacrylate) bromide (**P12PP**), where the side chains are terminated by a hydrogen-bond acceptor in close proximity to an ion pair, is mixed in equimolar proportion with a series of phenol-functionalized mesogenic complexants (***X***), some of which have highly polar tails, while others have chiral tails and most contain an azo moiety for potential optical responsiveness. It is found that, in all cases, hydrogen-bond complexation is successful and essentially complete, leading to supramolecular homopolymeric complexes **P(*X*)** with well-defined thermotropic LC characteristics. These complexes, which are partially crystalline initially, have above-ambient glass transitions and smectic LC mesophases that are monotropic, enantiotropic or effectively enantiotropic, depending on the molecular characteristics of ***X***. The presence of a polar tail hampers recrystallization after melting, with a cyano tail suppressing it completely and also strongly retarding the development of the LC mesophase from the isotropic phase. This might be related to enhanced electrostatic interactions and increased viscosity in the melt. The mesophase periodicity of **P12PP** is unchanged by complexants with a flexible alkyl tail, suggesting that they can adapt to the packing structure of **P12PP** (previously reported to be partial bilayer smectic A-like), whereas more rigid albeit shorter complexants lead to a periodicity increase (indicative of an effective single-layer smectic A mesophase). Possible molecular packing models are presented and discussed.

Introduction

The formation of organized assemblies via specific noncovalent interactions between complementary components to obtain various molecular architectures has been an important development in supramolecular chemistry in the last 2 decades.[1−3] This approach has also been used profitably in the design of supramolecular liquid crystal polymers (supra-LCPs).[4−8] Primary advantages of these materials are the relative ease and rapidity with which various functionalities of interest (for example, for potential applications as materials in information storage, molecular electronics, medicine, etc.) can be incorporated and new structures and properties (involving, for example, lability of the noncovalent bonds at higher temperatures) introduced.

Generally to date, the supramolecular link in a given supra-LCP system is of one type only, most often involving either hydrogen or ionic bonding between appropriate molecular species. To more fully realize the power and versatility of the supramolecular approach in materials design, it is desirable to investigate how a particular supramolecular linkage works in the presence of other potentially interfering interactions as well as the feasibility of employing two or more types of supramolecular linkages simultaneously.[4f,9] Among the few examples in the supra-LCP literature where this direction has been taken, our group investigated a tail-end pyridylpyridinium dodecyl methacrylate polyamphiphile (**P12PP**, Figure 1) to which a simple surfactant, 4-octylphenol, was successfully hydrogen-bonded (phenol−pyridyl) up to near-equimolar proportions without interference from the nearby ionic (pyridinium) groups, leading to thermotropic liquid crystallinity as a supramolecular side-chain LCP (supra-SCLCP).[10] Ikkala, Ruokolainen and coll. have shown that a serial noncovalent linkage involving both hydrogen and ionic bonding can associate pentadecylphenol to poly(4-vinylpyridine) (P4VP) via methane or toluene sulfonic acid in block copolymers of P4VP and polystyrene (the sulfonic acid protonates P4VP, and the phenol hydrogen-bonds to the resulting sulfonate group), giving thermally responsive hierarchical self-assembly of liquid crystal order within block copolymer order, as observed also with direct hydrogen bonding.[11,12]

Outside of the LCP literature, Nair and Weck demonstrated, using random comb copolymers of tail-end quaternary ammonium and tail-end 2,6-diaminopyridine functions, that it was possible to independently complex simple oppositely charged surfactants to the former counit by ionic bonding and *N*-butylthymine to the latter counit via a triple H-bond, whether proceeding sequentially or simultaneously.[13] In other words, the two types of interactions act orthogonally to each other in the systems studied.[13] This group also showed that the same hydrogen-bonding interaction and metal coordination (using Pd) act orthogonally in random and block copolymers.[14] On the other hand, Ikkala and coll. obtained evidence suggesting that the coordination of zinc dodecylbenzenesulfonate to dodecylbenzenesulfonic acid-doped polyaniline (DBSA-PANI) does not occur at the free aminic nitrogen sites, but instead at the already complexed sulfonate groups of DBSA-PANI via water-mediated

* To whom correspondence should be addressed. E-mail: geraldine.bazuin@umontreal.ca.

10.1021/ma070689t CCC: $37.00
Published on Web 06/23/2007

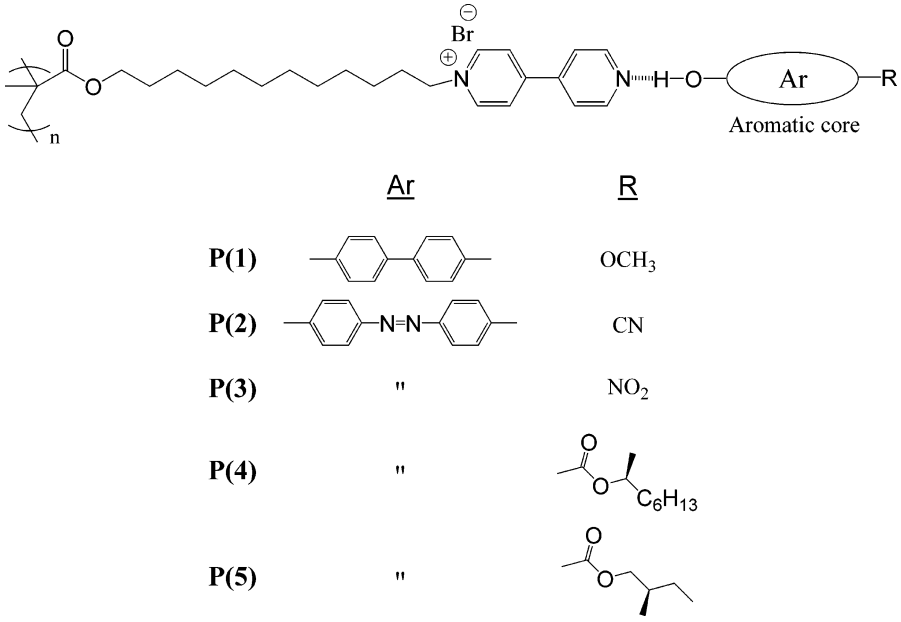

Figure 1. Hydrogen-bonded complexes **P(*X*)** composed of the polyamphiphile **P12PP** and (azo)phenol-functionalized small molecules ***X*** (***X*** = 1−5).

hydrogen bonds.[15] This case illustrates that supramolecular linkages can be interdependent and occur at unexpected or undesired sites. Thus, it is necessary to explore a much larger variety of systems than studied until now, especially more complex systems, to map out the specificity and independence or not of noncovalent linkages and combination of linkages in supramolecular assemblies.

Concerning supra-LCPs, many mesogenic motifs of practical interest for specific applications include moieties that constitute potential interference sites for the desired complexation, in particular highly polar units. In this context, the **P12PP** polyamphiphile mentioned above constitutes an ideal platform to test supramolecular assembly and LC behavior in conditions where there is what might be considered to be a soup of different interactions. The pyridylpyridinium functionality allows for both hydrogen-bonding and ionic complexation (as well as complexation through metal coordination), and it is a relatively simple matter to synthesize a variety of appropriately functionalized small molecules ("complexants") with desired chemical and mesogenic features. While our previous study[10] involving this polyamphiphile showed that hydrogen-bond complexation experiences no interference from the pyridinium groups, this was demonstrated using one of the simplest small-molecule complexants possible, an alkyl phenol, which presents only a flexible alkyl tail, and no polar moiety other than the phenol functionality through which the complexation takes place.

In the present contribution, we investigate a variety of phenol-functionalized mesogenic complexants (***X***) (Figure 1) of specific interest (indicated below), several of which have significant polarity, in particular highly polar tails. The latter constitute potential interference elements for the desired self-assembly, possibly in combination with the ionic groups of **P12PP**. Furthermore, the LC expression of the different mesogenic moieties in the complexes—i.e., the thermal and structural behavior of the potentially liquid crystalline supramolecular assemblies—may be influenced by the electrostatic environment, in particular the ionic groups possibly through dipole−dipole interactions. In this context, the mesogenic complexants ***X*** were chosen for a combination of reasons. First, it was desired that all five complexants be composed of mesogenic cores and tails of the type frequently found in all-covalent small-molecule and polymer liquid crystals. Moreover, except for **1**, they were chosen to be azo-based in view of the potential use of the complexes as photoresponsive materials and, consequently, the huge interest that azo-containing materials have long sustained and continue to sustain scientifically and technologically,[16] including in many supra-LCPs.[4,6−8] Two of these have short, highly polar tails (**2**, **3**) and two have nonpolar, flexible tails, one with a longer (**4**) and one with a shorter (**5**) alkyl moiety. These latter two, moreover, were chosen to be chiral for the possible generation of chiral mesophases (e.g., smectic C*). Complexant **1**, which possesses a short nonpolar tail, can be viewed as a rigid counterpart of the (nonpolar) octyl phenol complexant used in ref 10 (furthermore, it was readily available since it is an intermediate in the synthesis of surfactomesogens[17] used in other projects in our group[18]). An additional interest of employing more rigid complexants with and without polar tails vs complexants with flexible alkyl tails is related to the possible influence of these factors on the LC packing structure. In the polyamphiphile complexes investigated to date, all employing simple alkyl surfactants as complexants, it has been observed that there is a surprising insensitivity of the structural periodicity to the presence and length of the surfactant, either hydrogen bonded or ionically bonded.[10,19,20]

Architecturally, and by the type and placement of the noncovalent bond (far from the polymer backbone), these complexes resemble the large family of supra-SCLCPs investigated by Kato and coll., where a variety of pyridyl derivatives were hydrogen-bonded to various comb-like polymers with carboxylic acid terminal groups in the side chains.[4b,g] In contrast to our complexes, none of their systems contain ionic groups, and from the point of view of supramolecular synthesis they are therefore more straightforward. For this reason, in the cases where similar mesogenic cores are employed, they will also provide a convenient comparison for our complexes, especially for evaluating the effect of the electrostatic environment on the LC behavior. It may be added that the presence of ionic moieties can be a desirable feature in real applications, in particular because they will certainly modify the viscoelastic properties of these materials, most simply by mitigating the effect of side-chain plasticization on the glass transition temperature, but also by giving a higher melt viscosity; this can be beneficial, for

Table 1. Thermal Data[a] of the Small Molecules (*X*), Determined by DSC and TGA[36]

	1	**2**	**3**	**4**	**5**	**5′** [b]
T_m/°C (ΔH/J·g^{-1})	184 (180)	207 (140)	220[c] (150)	96 (100)	120 (60)	116 (90)
T_m/°C (literature)	182−184[23]	200−204[25]	219−221[26]		113−115[27]	112−113[24]
T_{cr}/°C (ΔH/J·g^{-1})	173 (−170)	196 (−120)	180 (−120)	*d*	102 (−70)	100 (−90)
$T_d^{2\%}$ (°C)	160	188	197	206	180	

[a] T_m: melting point. T_{cr}: crystallization temperature; ΔH: transition enthalpy. $T_d^{2\%}$: 2% weight loss temperature. [b] Same compound as **5** but without the N═N moiety. Data obtained from ref 28. [c] 195 °C on second and third heating scans (limited to 210 °C); first scan agrees with literature value.[26] [d] No crystallization was observed during cooling, but a recrystallization endotherm occurs at about 50 °C in subsequent heating.

example, for use of these materials as anisotropic glasses.[20] The present series, to our knowledge, constitutes one of the rare studies in the literature that investigate LC properties of *ion-containing* polymer complexes based on hydrogen-bonding, although there are a few studies on such small-molecule complexes.[21,22]

Experimental Section

Materials. 4-Aminobenzonitrile (98%), 4-nitroaniline (99+%), sodium nitrite (Reagent Plus 100%), 4-nitrobenzoyl chloride (98%), (*S*)-2-octanol (99%), (*S*)-2-methyl-1-butanol (99%), 4-dimethylaminopyridine (99%), tin(II) chloride $SnCl_2$ (98%), and phenol (99%) were all used as received from Aldrich. Dichloromethane and pyridine were dried by distillation from calcium hydride and sodium metal, respectively, and stored over 4-Å molecular sieves. Water used for polymerization, dialysis and azobenzene synthesis was purified by a Milli-Q system (resistance 18 MΩ). Column chromatography was performed using silica gel (60 Å, 70−230 mesh, Aldrich).

Techniques of Analysis. NMR spectra were recorded on a Bruker Avance 400 MHz spectrometer. Chemical shifts are given in ppm using the residual solvent signal ($CDCl_3$, DMSO-d_6, acetone-d_6, CD_3OD) as an internal reference. The melting points were measured on a Bibby Sterilin SMP10 melting point apparatus using capillary tubes. Fourier transform infrared (FTIR) spectra were recorded, mainly at ambient temperature, using a Varian (Digilab) FTS 3100 HE Excalibur spectrophotometer equipped with a DTGS detector; spectra at higher temperatures were obtained using a Pike temperature controller and cell assembly. The as-prepared samples were pressed into KBr pellets that were subsequently dried at 60 °C in vacuo for 24 h. UV−visible measurements of the azobenzene derivatives (**2**−**5**) were performed at ambient temperature in spectrometric grade CH_2Cl_2 (Aldrich) solutions at a concentration of 3.5×10^{-5} mol·L^{-1} using a Cary 500 spectrometer and an analysis cell with an optical path length of 10 mm.

Thermogravimetric analysis (TGA) was carried out under nitrogen flow at a heating rate of 10 °C/min to 500 °C using a TA Instruments Hi-Res TGA 2950 analyzer. The samples were dried in situ at 100 °C for 5 min just prior to the heating scan. The temperature of thermal degradation ($T_d^{2\%}$) was measured at the point of 2% weight loss relative to the weight at 100 °C. Differential scanning calorimetry (DSC) was carried out using a Perkin-Elmer DSC-7 calorimeter, calibrated by indium, flushed with nitrogen and cooled by dry ice. Samples of 10−15 mg were crimped in standard aluminum pans. Heating and cooling rates were 10 °C/min. First-order transitions were taken at the maximum point of endothermic or exothermic peaks and the glass transition temperature (T_g) at the midpoint of the heat capacity jump. Polarizing optical microscopy (POM) was performed using a Zeiss Axioskop 40Pol microscope using 10× and 40× objectives and a QImaging MicroPublisher 3.3RTV camera. The temperature was regulated by a Linkam Scientific Instrument THMS600 hot stage and a TMS94 temperature controller.

X-ray diffraction (XRD) studies were carried out with a Bruker diffractometer (D8 Discover), using Cu Kα radiation (λ = 1.542 Å). The diffraction pattern was recorded with a Bruker AXS two-dimensional wire-grid detector. Samples were packed into 1.0 mm diameter capillary tubes (Charles Supper). The sealed capillaries were placed in an Instec HCS410 heating stage, coupled with an Instec STC200 temperature controller. 1-D data were obtained by integrating the 2-D data. The *d*-spacings were determined from the maximum of the diffraction peaks according to the Bragg equation, $n\lambda = 2d(\sin\theta)$, where n is an integer giving the order of the diffraction peak, θ is the angle of incidence, and λ is the wavelength of the X-ray beam used. The Bragg spacings determined from the small-angle X-ray data were compared with the molecular lengths calculated with the aid of Hyperchem 5.0 (Hypercube), assuming most extended conformations and including van der Waals' radii at the extremities. The hydrogen bond length was taken to be 2.8−3.0 Å.

Table 2. Wavelength (λ_{max}) and Intensity (ϵ) of Maximum Absorption in the UV−Visible Spectra of the Azo-Containing Small Molecules (*X*) in CH_2Cl_2 Solution

	2	**3**	**4**	**5**
λ_{max} (nm)	356	369	352	352
$\epsilon \times 10^{-2}$ (L·mol^{-1}·cm^{-1})	265	262	248	265

Synthesis. The syntheses of most of the phenol-functionalized compounds used as complexants have been reported in the literature previously (as indicated below for each compound), often because they are intermediates for other compounds. Thus, the specific procedures used by us are described very briefly, and mainly analytical data are given. Melting points (which are the same by DSC and melting point apparatus within ±1 °C) and their comparison with literature values, as well as crystallization temperatures and transition enthalpies (determined by DSC) and degradation temperatures (determined by TGA) are given in Table 1.

4′-Methoxybiphenyl-4-ol (1).[18,23] White solid (32% yield). ^{1}H NMR ($CDCl_3$): δ = 3.85 (s, 3H, OCH_3), 4.9 (s, 1H, OH), 6.85 (d, 2H, Ar−OH), 6.95 (d, 2H, Ar−OMe), 7.40 (d, 2H, Ar), 7.45 (d, 2H, Ar). ^{13}C NMR ($CDCl_3$): δ = 55.8, 114.6, 115.9, 128.1, 128.3, 133.8, 134.2, 155, 157.3. IR (cm^{-1}): 3421, 3373, 3016, 2954, 2835, 1610, 1598, 1501, 1378, 1249, 1178, 1038, 817, 793. Anal. Calcd for $C_{13}H_{12}O_2$: C, 77.98; H, 6.04. Found: C, 77.87; H, 6.07.

Azobenzene Compounds, General Procedure. The azobenzene compounds were synthesized via a diazonium reaction with phenol on the appropriate aniline derivative [**2** and **3** are commercially available; **4** and **5** were synthesized by reacting 4-nitrobenzoyl chloride with a chiral alcohol (giving **4a** and **5a**, described below), followed by reduction (giving **4b** and **5b**, described below)]. To a suspension of the *p*-substituted aniline derivative (20 mmol) in 50 mL of 2 M HCl solution cooled to −5 °C in a NaCl ice−water bath was added $NaNO_2$ (27 mmol) in small portions at a time. After stirring for 10 min, the resulting diazonium salt solution was added dropwise to a solution of phenol (20 mmol) in 50 mL of 2 M NaOH solution at −5 °C. The reaction mixture was stirred for 4 h at 0−5 °C and then acidified with 2 M HCl and warmed to room temperature. The precipitate was filtered, washed several times with distilled water, dried in vacuo and purified by column chromatography on silica gel using dichloromethane as eluent. The UV−visible spectra of these compounds show a single, approximately symmetric band; the salient data are presented in Table 2.

4-(4′-Cyanophenylazo)phenol (2).[25] Red solid (87% yield). ^{1}H NMR (acetone-d_6): δ = 7.10 (d, 2H, Ar−O), 7.80−8.10 (m, 6H, Ar−N═ and Ar−CN), 9.35 (s, 1H, OH). ^{13}C NMR (acetone-d_6): δ = 113.4, 116.5, 118.6, 123.3, 126, 133.8, 146.6, 155.2, 162.2. IR (cm^{-1}): 3307, 3216, 2240, 1606, 1586, 1503, 1461, 1351, 1280, 1214, 1189, 1137, 1104, 847. Anal. Calcd for $C_{13}H_9N_3O$: C, 69.95; H, 4.06; N, 18.82. Found: C, 70.14; H, 4.02; N, 18.95.

4-(4′-Nitrophenylazo)phenol (3).[26] Red solid (68% yield). ^{1}H NMR (acetone-d_6): δ = 7.10 (d, 2H, Ar−O), 7.90 (d, 2H, Ar−N═), 8.10 (d, 2H, Ar−N═), 8.45 (d, 2H, Ar−NO_2), 9.45 (s, 1H, OH). ^{13}C NMR (acetone-d_6): δ = 116.4, 123.4, 125.2, 126.2, 146.8, 148.7, 156.4, 162.4. IR (cm^{-1}): 3430, 3113, 2963, 1604, 1586, 1504, 1458, 1336, 1284, 1140, 1109, 863, 850. Anal. Calcd for $C_{12}H_9N_3O_3$: C, 59.26; H, 3.73; N, 17.28. Found: C, 59.09; H, 3.82; N, 17.38.

(*S*)-Octan-2-yl-4-(4′-hydroxyphenylazo)benzoate (4). Orange solid (50% yield). ^{1}H NMR (acetone-d_6): δ = 0.90 (t, 3H, CH_2CH_3), 1.25−1.55 (m, 11H, $CHCH_3$ and 4 × CH_2), 1.60−1.90 (m, 2H, $CHCH_2$), 5.20 (se, 1H, *CH*CH3), 7.10 (d, 2H, Ar−O), 7.85−8.05 (m, 4H, Ar−N═), 8.25 (d, 2H, Ar−CO), 9.3 (s, 1H, OH). ^{13}C NMR (acetone-d_6): δ = 13.8, 19.7, 22.7, 25.6, 31.9, 36.3, 72, 116.4, 122.7, 126, 131.1, 132.4, 146.8, 155.5, 161.8, 165.8. IR (cm^{-1}): 3363, 2956, 2923, 2856, 1675, 1604, 1595, 1506, 1436, 1348, 1307, 1279, 1227, 1138, 1121, 843. Anal. Calcd for $C_{21}H_{26}N_2O_3$: C, 71.16; H, 7.39; N, 7.90. Found: C, 70.98; H, 7.58; N, 7.79.

(*S*)-2-Methylbutyl-4-(4′-hydroxyphenylazo)benzoate (5).[27] Orange solid (60% yield). ^{1}H NMR (acetone-d_6): δ = 0.95 (t, 3H, CH_2CH_3), 1.05 (t, 3H, $CHCH_3$), 1.25−1.65 (m, 2H, $CHCH_2$), 1.95 (m, 1H, *CH*CH3), 4.10−4.30 (m, 2H, OCH_2), 7.05 (d, 2H, Ar−O), 7.90−8.05 (m, 4H, Ar−N═), 8.25 (d, 2H, Ar−CO), 9.3 (s, 1H, OH). ^{13}C NMR (acetone-d_6): δ = 11.7, 16.4, 26.4, 34.5, 69.6, 116.3, 122.9, 125.8, 130.7, 131.8, 146.8, 155.5, 161.9, 165.9. IR (cm^{-1}): 3402, 2965, 2877, 1690, 1607, 1588, 1506, 1463, 1352, 1302, 1284, 1215, 1137, 864. Anal. Calcd for $C_{18}H_{20}N_2O_3$: C, 69.21; H, 6.45; N, 8.97. Found: C, 69.54; H, 6.40; N, 8.94.

(*S*)-Octan-2-yl-4-nitrobenzoate (4a). To a solution of (*S*)-2-octanol (0.5 g, 3.84 mmol) in 10 mL of dry CH_2Cl_2 were successively added pyridine (0.5 g, 6.33 mmol), 4-nitrobenzoyl chloride (1 g, 5.38 mmol) and 4-dimethylaminopyridine (44 mg, 0.36 mmol). After being stirred for 5 h at room temperature, the mixture was filtered over $MgSO_4$. The solvent was removed and the resulting residue was chromatographed on silica gel (1/1 dichloromethane/hexane as eluent) to yield a yellow liquid (1.03 g, 96% yield). ^{1}H NMR ($CDCl_3$): δ = 0.90 (t, 3H, CH_2CH_3), 1.10−1.50 (m, 11H, $CHCH_3$ and 4 × CH_2), 1.60−1.90 (m, 2H, $CHCH_2$), 5.20 (se, 1H, *CH*CH3), 8.20 (d, 2H, Ar−CO), 8.30 (d, 2H, Ar−NO_2).

(*S*)-2-Methylbutyl-4-nitrobenzoate (5a). Using the same procedure as described for **4a**, compound **5a** (yellow liquid) was obtained in 92% yield. ^{1}H NMR ($CDCl_3$): δ = 0.95 (t, 3H, CH_2CH_3), 1.05 (t, 3H, $CHCH_3$), 1.30−1.60 (m, 2H, $CHCH_2$), 1.95 (m, 1H, *CH*CH3), 4.15−4.35 (m, 2H, OCH_2), 8.20 (d, 2H, Ar−CO), 8.30 (d, 2H, Ar−NO_2).

(*S*)-Octan-2-yl-4-aminobenzoate (4b). To a solution of $SnCl_2$ (3.45 g, 18.2 mmol) in 20 mL of ethanol under nitrogen was added dropwise **4a** (1 g, 3.58 mmol) in 10 mL of ethanol. The mixture was stirred at reflux for 2 h. After cooling, the solution was poured into 100 mL of ice−water and alkalized to a pH of 7−8 with a small amount of K_2CO_3. The product was extracted with diethyl ether (4 × 300 mL). The organic layer was washed with brine solution, dried over Na_2SO_4 and concentrated. The product was purified by silica column chromatography (1/1 dichloromethane/hexane as eluent) to give **4b** as a yellow solid (0.78 g, 88% yield); mp 82 °C. ^{1}H NMR (DMSO-d_6): δ = 0.85 (t, 3H, CH_2CH_3), 1.20−1.40 (m, 11H, $CHCH_3$ and 4 × CH_2), 1.50−1.70 (m, 2H, $CHCH_2$), 4.95 (se, 1H, *CH*CH3), 5.95 (s, 2H, NH_2), 6.55 (d, 2H, Ar−N), 7.60 (d, 2H, Ar−CO). ^{13}C NMR (DMSO-d_6): δ = 14.8, 21, 22.9, 25.8, 29.3, 32.1, 36.2, 70.5, 113.3, 117.4, 131.6, 154, 166.1.

(*S*)-2-Methylbutyl-4-nitrobenzoate (5b). Using the same procedure as described for **4b**, compound **5b** (yellow solid) was obtained in 87% yield; mp 51 °C. ^{1}H NMR (DMSO-d_6): δ = 0.90 (t, 3H, CH_2CH_3), 0.95 (t, 3H, $CHCH_3$), 1.15−1.60 (m, 2H, $CHCH_2$), 1.75 (m, 1H, *CH*CH3), 3.90−4.15 (m, 2H, OCH_2), 5.85 (s, 2H, NH_2), 6.55 (d, 2H, Ar−N), 7.65 (d, 2H, Ar−CO). ^{13}C NMR (DMSO-d_6): δ = 12.1, 17.3, 26.6, 34.7, 68.6, 113.3, 116.9, 131.8, 154.2, 166.8.

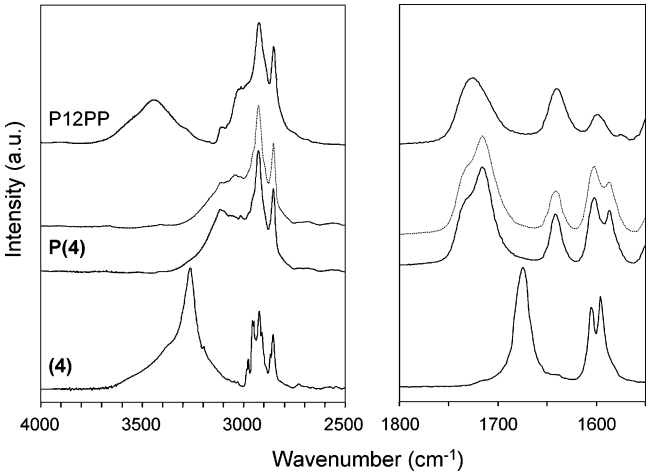

Figure 2. Ambient temperature FTIR spectra, in selected wavenumber regions, of the complex **P(4)** and the two pure components **P12PP** and **4**. The solid and dotted lines for **P(4)** give the spectra before and after exposure to 150 °C, respectively.

Polymer Synthesis and Preparation of the Complexes. A single batch of the polyamphiphile, **P12PP**, was synthesized according to the procedure described previously.[10,28] The polymerization conditions, which include the use of transfer agent, were chosen with the aim of obtaining a low molecular weight (oligomer range) polymer in order to have a soluble polymer to facilitate complexation, previous studies having indicated that solubility is limited for higher molecular weights.[19,29] After polymerization of the monomer in aqueous micellar conditions [using the sodium salt of 4,4′-azobis(4-cyanovaleric acid) (ACVA) as initiator and 1-dodecylmercaptan (DM) as transfer agent], purification by dialysis (using a VWR Spectrapor membrane with a molecular weight cutoff of 3500) and solvent removal, **P12PP** was obtained with a molecular weight of 9200[30] (dp = 19) [as estimated from the polymer repeat unit signals (e.g., CH_2−O at 4.15 ppm) in comparison to the CH_2−S signal at 2.6 ppm from the chain-end DM fragment (and, with less precision, the partially overlapped CH_2 signal at 2.2 ppm from the chain-end ACVA fragment) in the ^{1}H NMR spectrum of **P12PP** in CD_3OD, assuming one chain transfer fragment per chain].

To prepare the complexes **P(*X*)** (***X*** = 1 to 5) equimolar quantities of the two components were dissolved separately at room temperature in ethanol (2 mmol in 20 mL), then the small molecule solution was added all at once to the polyamphiphile solution. The resulting clear solution was stirred for 3−4 days at room temperature, followed by solvent evaporation. All the complexes were dried under vacuum at 60 °C for at least 2 days and then kept under vacuum at room temperature until analysis.

Results and Discussion

Infrared Analysis. Fourier transform infrared spectroscopy (FTIR) was used to verify that complexation between **P12PP** and each of the small molecules (***X***) in the complexes, **P(*X*)**, takes place. It will be shown that hydrogen bonding between the phenol and pyridyl functions, which are in equimolar proportion, is essentially complete. It is concluded from this that neither the ionic interactions nor potential dipolar interactions between ion pairs in **P12PP** and polar groups in ***X*** interfere with the desired supramolecular linkage. Furthermore, this linkage appears stable into the isotropic state.

A representative example is illustrated in Figure 2, where the FTIR spectrum of the complex, **P(4)**, is compared with those of the two pure components in the 4000−2500 and 1800−1550 cm^{-1} regions. It is observed that the broad absorption band centered at about 3440 cm^{-1} in the spectrum of **P12PP** (attributed to adsorbed water[10]) and the strong absorption band centered at 3263 cm^{-1} in **4** are absent in the spectrum of **P(4)**

Table 3. Wavenumbers of Maximum Absorption in the OH Stretching Vibration Region in the FTIR Spectra of the Small Molecules (*X*) and the Complexes P(*X*)

	1 or **P(1)**	**2** or **P(2)**	**3** or **P(3)**	**4** or **P(4)**	**5** or **P(5)**
X: ν_{OH} (cm^{-1})	3421, 3373	3307	3430	3263	3402
P(*X*): ν_{OH} (cm^{-1})	~3100	~3100	~3100	~3100	~3100

and replaced by an absorption band around 3100 cm^{-1}. As indicated in Table 3, similar observations were made for each of the complexes in comparison to their constituents (see Supporting Information and ref 31).

The shift of the hydroxyl stretch to lower wavenumbers in the complexes is diagnostic of hydrogen-bonding of phenol to pyridyl.[10,32] This shift appears similar for each of the complexes studied—i.e., near 3100 cm^{-1}—whereas, by comparison, it is found near 3180 cm^{-1} for the octylphenol/**P12PP** complex,[10] thus indicating a stronger hydrogen bond[33] for the present complexes, probably due to the greater acidity of the phenol moiety imparted by the (azo)phenyl substituents.[34] The fact that the spectra of all of the complexes are essentially absorption-free in the region above 3300 cm^{-1} [as shown in Figure 2 for **P(4)** and in the Supporting Information for the others] indicates that the hydrogen-bonding is essentially complete in these (equimolar) complexes.

Changes in other regions of the spectra also occur, but are difficult to interpret in detail due to overlapping bands. This is shown in the 1550−1800 cm^{-1} region in Figure 2 for **P(4)** in particular. First, the overlapping pyridyl absorption bands of **P12PP** and the phenyl-related bands of **4** are evidently modified in the complex. Second, it is of interest to note that the carbonyl stretching vibration of **4**, located at 1675 cm^{-1}, is shifted to higher wavenumbers in **P(4)**. This was observed also for **5**, for which the carbonyl stretch before complexation is located at 1690 cm^{-1} (1680 cm^{-1} for the same molecule without the azo group[35]). The low position of the carbonyl band in the small molecules is probably caused by hydrogen bonding between the hydroxyl and ester carbonyl groups in these molecules that is broken by their complexation with **P12PP**. The carbonyl absorption of **P12PP** also appears to shift in **P(4)** and **P(5)**, such that there are (at least) two carbonyl bands located on either side of the position observed in **P12PP** alone. In the other complexes, the **P12PP** carbonyl band is not modified.

It was verified that the spectra of complexes exposed to 150 °C undergo little change compared to the initial spectra (see Figure 2 and Supporting Information). In addition, a series of spectra of **P(2)** (given in the Supporting Information) were taken at various temperatures up to 140 °C (heating and cooling), and no significant changes were observed—in particular, in the bands reflecting complexation and in the cyano band at 2226 cm^{-1}. This indicates that the hydrogen bond is stable over the whole temperature range of interest, although possibly labile at higher temperatures.

Thermal Behavior. First, the thermal stability of the complexes was determined by TGA. As shown in Table 4, they all have 2% weight loss values ($T_d^{2\%}$) between 185 and 215 °C. This is in the same range as that for the uncomplexed polyamphiphile, **P12PP**, and those for the small molecules alone (Table 1) [except for **1** whose 2% weight loss occurs about 45 °C below that of **P(1)**]. Subsequent analyses of the complexes were restricted to temperatures well below their $T_d^{2\%}$, thus assuring that neither degradation nor potential loss of small molecule occurs.

As a point of reference for the complexes, it was noted that the small molecules (***X***) all possess a crystalline phase that melts and crystallizes directly to and from the isotropic phase (as determined by POM, DSC and XRD), and no crystal−crystal transitions were observed by DSC. Their melting points range from 95 to 220 °C (Table 1) with high transition enthalpies, and crystallization occurs with mild supercooling (10−20 °C).[36] The most stable crystalline phases (i.e., those with the highest melting points) are observed for the compounds with polar tails, CN and NO_2, and the least stable for those with the (chiral) alkyl tails. Interestingly, compound **(4)**, which has a relatively long (chiral) alkyl tail and the lowest melting point, shows no crystallization during cooling but instead crystallizes at about 50 °C during subsequent heating (as observed by DSC). The polymer **P12PP** is noncrystalline, and the only transition observed by DSC is a glass transition, which is located at a much higher temperature than analogous polymers with no ionic groups present.[29]

Table 4. Thermal Data (TGA and DSC) of P12PP and the Complexes P(*X*)[a]

sample	$T_d^{2\%}$ (°C)	T_g (°C)	T_m/T_{cr} (ΔH) [°C (J/g)]	T_{LC-is} (ΔH) [°C (J/g)]
P12PP	201	83		
P(1)	205	43	134 (20)	
			79 (−9)	*88 (−2)*
P(2)	202	52	107−111 (~10)[b]	76−80 (~2)[b]
				65−71 (−2)
P(3)	212	46	123 (18)[b]	87 (3)[b]
				78 (−3)
P(4)	198	37	106 (8)[c]	119 (2)
				109 (−2)
P(5)	187	41	128 (21)	~132[d]
			91 (−12)	*121 (−3)*
P(5′)[e]		36	131 (22)	~135[d]
			97 (−15)	*125 (−2)*

[a] $T_d^{2\%}$, temperature of 2% weight loss; T_g, glass transition temperature (from second and third heating scans); T_m, melting point; T_{cr}, crystallization temperature (cooling scans); T_{LC-is}, liquid crystal−isotropic transition temperature; ΔH, transition enthalpy. *Italicized data are from cooling thermograms.* [b] T_m observed in first heating scan only; T_{LC-is} observed after melting only (i.e., after first heating scan). Repeated scans of **P(2)** following the first are reproducible for a given sample, but vary somewhat from sample to sample. [c] Recrystallization takes place at about 70 °C in the heating scan following cooling. [d] In the form of a shoulder on the high-temperature side of the melting peak (enthalpy included in that for T_m). [e] This complex is formed with a compound identical to **5** but without the N═N moiety.[28,35]

The thermal characteristics of the complexes are shown by the DSC thermograms given in Figure 3, with the corresponding transition temperatures and enthalpies listed in Table 4. Since the first heating curves are frequently different from the subsequent ones (as will be addressed below), both the first and an example of a subsequent heating curve are shown in Figure 3 along with a cooling curve. In all cases, the second and following heating curves as well as the cooling curves are reproducible. The phases are identified by XRD (described in the next section) aided by POM.

The complexes all show a clear glass transition, which lies between 35 and 55 °C (with a heat capacity increment of about 0.3 $J \cdot K \cdot g^{-1}$) compared to 83 °C for **P12PP**. This reflects a plasticization effect that can be expected from an effective increase in the polymer side-chain length due to complexation by the small molecule. The lowest T_g's are obtained for **P(4)** and **P(5)**, which can be related to the flexible alkyl tail of **4** and **5**, and the highest T_g's are obtained for **P(2)** and **P(3)**, which can be attributed to the polar tail and greater rigidity of **2** and **3**. Thus, the trend in the T_g of the complexes relative to molecular characteristics parallels the (much stronger) trend observed for the melting points of the small molecules.

It may be noted that there appears to be a weak T_g-like transition near 65 °C in the second and subsequent heating

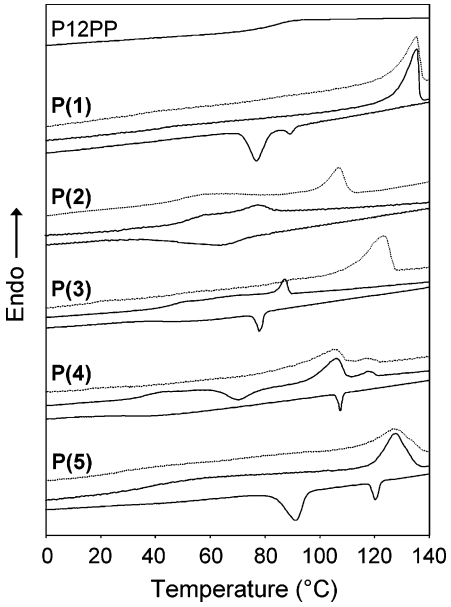

Figure 3. DSC thermograms of **P12PP** and the complexes **P(*X*)** (dotted lines, initial heating; solid lines, second and third heating and cooling).

thermograms for **P(3)**. This is worth mentioning because the presence of what appears to be two T_g's is occasionally reported in the literature for comb-like polymers,[37,38] including for an analogous pyridinium polyamphiphile in which the Br counterion is substituted by butyl- and octylsulfonate counterions,[19] and has been attributed to cooperative long-range motion involving the polymer main chain and side chains, respectively.

In contrast to **P12PP**, the complexes all possess a crystalline phase initially (see XRD data below). Their melting points (as observed in the initial heating DSC scans) are similar, ranging in temperature from 105 to 135 °C, and do not seem to follow any particular trend relative to the molecular characteristics except for **P(4)** having a lower melting point than **P(5)**, which can be related to the longer alkyl tail of the former (see below). Compared to the corresponding small molecules, the melting points of **P(4)** and **P(5)** are a little higher, which argues against their being due to uncomplexed ***X***. This argument—in accordance with the FTIR data above and with XRD data (see below)—can be extended to the other complexes even though their melting points are much lower than those of the corresponding small molecules. The relatively small variation in melting point can thus be attributed to the similarity in molecular architecture of the complexes. It is also noted that the melting points are fairly broad, and the enthalpies not very high [in particular for **P(2)** and **P(4)**] suggesting partial crystallinity.

For **P(1)**−**P(3)**, melting proceeds directly into the isotropic phase (as observed by POM). However, for **P(4)**, it is followed by a liquid crystal mesophase (fluid and birefringent in POM), with about a 15 °C stability interval before reaching the isotropic phase. For **P(5)**, in comparison, a weak shoulder can be detected on the high-temperature side of the melting peak, suggestive of a liquid crystal phase over a narrow temperature range, which is confirmed by POM.

On cooling, all of the complexes display a DSC transition from the isotropic to a liquid crystal phase. This transition is very well-defined for **P(3)**−**P(5)**, appearing in order of temperature as **P(5)** > **P(4)** > **P(3)**. For **P(2)**, it is very broad and occurs at a somewhat lower temperature still. Only **P(1)** and **P(5)** crystallize during cooling, such that the second and subsequent heating thermograms for these two complexes are very similar to the initial one. Thus, the liquid crystal phase in **P(1)** is monotropic[39] with a thermal stability of only about 10 °C during cooling, whereas that of **P(5)** is enantiotropic (given its appearance over a short temperature interval between melting and isotropization) and has a 30 °C stability range during cooling. It is noteworthy that almost identical behavior to that of **P(5)** was noted for a **P12PP** complex where the small molecule lacks the N═N moiety [annotated as **P(5′)** in Table 4; see Table 1 for **5′**].[28] On the other hand, **P(4)** like **(4)** shows a recrystallization endotherm during subsequent heating, located at about 70 °C, after which the thermogram is very similar to that for the first heating. The longer alkyl tail of **4** compared to that of **5** and/or the location of the branch point (chiral center) next to the ester link thus hampers crystallization in addition to destabilizing the crystal and liquid crystal phases somewhat [lower melting point and lower T_{LC-is} for **P(4)**], as is common in liquid crystals.[40]

For **P(2)** and **P(3)**, for which no crystallization takes place during cooling, none takes place either during subsequent heating, nor after 2 weeks at ambient temperature or 24 h at 70 °C. After 2 weeks at 70 °C, **P(3)** but not **P(2)** showed a very small amount of crystallization (as observed by XRD).[41] The suppression of crystallization renders at least **P(2)** an effective enantiotropic liquid crystal material. Without crystallization, the liquid crystal−isotropic transition in **P(2)** and **P(3)**, which takes place at a lower temperature than melting of the initial crystalline phase, is observed in the second and following DSC heating thermograms. It is clearly defined for **P(3)**, but is broad for **P(2)** (as during cooling). Their lower transition temperatures compared to those of **P(4)** and **P(5)** indicate that the presence of the polar tail reduces the thermal stability of the mesophase (relative to the isotropic phase) in these complexes. This contrasts with the non-ion-containing complexes of a polyacrylate-based comb polymer with benzoic acid terminal groups that are hydrogen-bonded to pyridyl-functionalized small molecules (stilbazole derivatives), where higher isotropization temperatures were observed for pyridyl derivatives with polar tails compared to those with alkoxy tails.[42] It also contrasts with what is often observed for cyano vs methoxy tails in all-covalent SCLCPs,[42,43] noted as well in tail-end pyridinium polyamphiphile analogues of **P12PP**.[29] Furthermore, both the nonionic hydrogen-bonded complexes and all-covalent SCLCP's generally show reversible ordered or crystalline phases for longer alkyl spacers (11−12 methylene units) including those with polar tails on the mesogenic core.[42,43]

This suggests that the combination of the polar tails and ionic groups in the complexes of the present study is responsible for the reduction in mesophase stability and for interference with crystallization. For **P(2)**, it may be responsible as well for the broadening of the liquid crystal−isotropic transition. This might be attributed to increased melt viscosity slowing down the crystallization kinetics drastically, as a result of the combined effects of electrostatic interactions among the pyridinium bromide ion pairs of the polymer side chain and among the polar tails of the complexant. Additionally, there may be (transient) dipolar interactions between the polar tails and pyridinium moieties in the melt—possibly facilitated by hydrogen-bond lability at higher temperatures—that impede reorganization upon cooling. Such interactions may also explain the reduced thermal stability of the mesophase of **P(2)** and **P(3)** compared to **P(4)** and **P(5)**.

Typical POM textures of the liquid crystal phases in the complexes are illustrated in Figure 4 (the photomicrographs were taken at ambient temperature after slow cooling from the isotropic phase, with no change detected in cases of crystal-

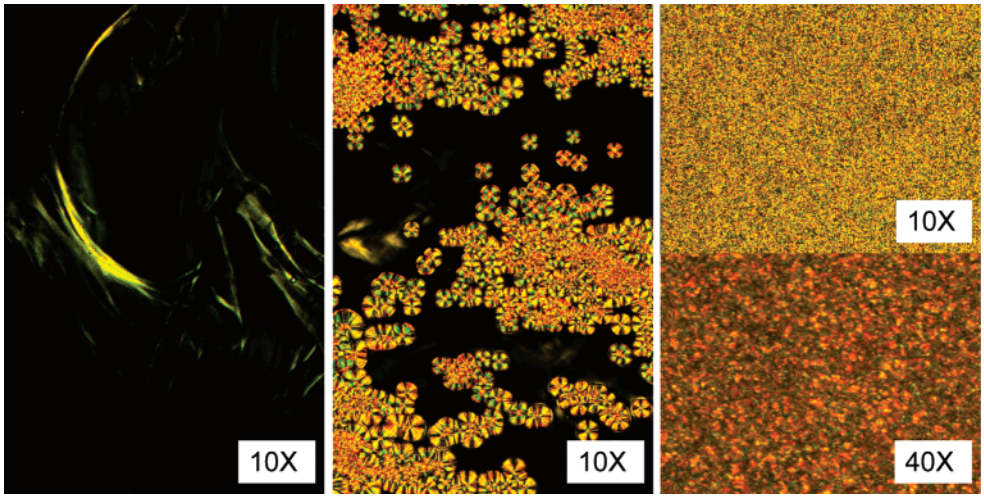

Figure 4. Typical POM textures observed for the complexes indicated, after cooling from the melt (objective size given in insets).

lization). The texture shown for **P(4)** was also obtained for **P-(5)** and **P(1)** [except with a bluish tint for **P(1)**]. **P(2)** showed almost no birefringence immediately after cooling, concordant with XRD data indicating poorly developed mesophase domains (see later). After a few days at ambient or after annealing near 70 °C, the birefringence increased only a little, although XRD indicated improved mesophase formation (see later), suggesting that the mesophase domain sizes are below the wavelength of light.

Structural Analysis. The X-ray diffractograms of the various complexes at temperatures corresponding to the different phases delimited by DSC analysis are shown in Figure 5. The corresponding Bragg spacings, d_B, calculated from the low-angle diffraction peaks are given in Table 5. The as-prepared complexes at ambient temperature (Figure 5a) were all partially crystalline, as indicated by the weak wide-angle diffraction peaks superimposed on a broad halo. After melting and cooling back to ambient temperature, during which a series of isothermal diffractograms were taken at various temperatures, **P(1)**, **P(4)**, and **P(5)** returned to the same crystalline form as before melting (Figure 5d). For **P(4)**, the occurrence of crystallization, in contrast to what was observed during the DSC scans, is attributed to the stepwise cooling rate (in particular, a diffractogram was recorded precisely in the range where the recrystallization endotherm is found in the DSC heating scan); another diffractogram was taken after cooling from the melt to ambient at a rate of 10 °C/min, which did not result in crystallization (dotted line in Figure 5c). **P(2)** and **P(3)** did not recrystallize after melting and stepwise cooling, and only **P(3)** showed a very small amount of crystallinity after annealing for 2 weeks at 70 °C (dotted line in Figure 5d). The diffractograms indicate that **P(4)** and **P(5)** [as well as **P(5′)**[28]] appear to have an essentially identical crystalline packing structure, which may be related to the presence of the alkyl tail. At low angles, these complexes as well as **P(1)** show an intense low-angle diffraction peak and a weaker second-order peak with reciprocal spacings of 1:2, consistent with a lamellar structure. **P(2)** and **P(3)** give more complex low- and wide-angle patterns before melting, as will be further commented below.

The XRD diffractograms of the complexes are very different from those of the corresponding small molecules in their crystalline phase (see Supporting Information). The diffractogram of **1** indicates that it possesses an orthogonal bilayer lamellar crystalline structure [four diffraction orders giving a Bragg spacing of 23 Å, or twice the molecular length (Table 5)]. The crystalline structures of the other small molecules do not appear to be lamellar, and the largest Bragg spacing observed in each case is 10 Å or less—thus much smaller than a molecular length. It is especially significant that none of the small molecules give diffraction peaks in the same lower angle region as do the complexes, for which the Bragg spacings are all above

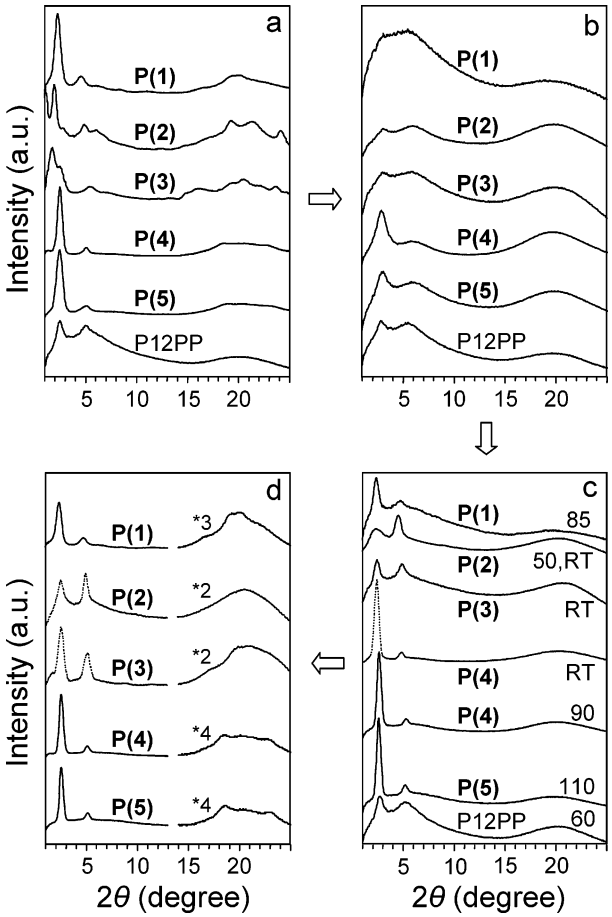

Figure 5. XRD profiles of the complexes **P(*X*)**: (a) at ambient temperature before melting; (b) in the isotropic state (~140 °C); (c) in the liquid crystal state at the temperatures indicated (in °C) [for **P(4)** at ambient (room temperature, RT): after cooling from the melt at 10 °C/min]; (d) following return to ambient temperature [for **P(2)**: after 1 day at ambient (similar after 2 weeks at 70 °C); for **P(3)**: after 2 weeks at 70 °C]. The wide-angle regions in part d are expanded relative to the lower angle region by the factor indicated. The arrows indicate the order in which the diffractograms with solid lines were taken. Profiles for **P12PP** at different temperatures are added for comparison.

Table 5. Bragg Distances (d_1, d_2) at Various Temperatures and Most Extended Molecular Lengths (l_C) Determined for P12PP and the Complexes P(*X*)[a]

sample	temp (°C)	state	d_1 (Å)	$2d_2$ (Å)	l_C[b] (Å)
P12PP	RT	*c*	35	35	28
	100		33	33	
	140		31	32	
P(1)	RT → 100	Cr	38	39	+12
	140 → 100	is	∼30	∼30	
	85	LC	37	37	
	70 → RT	Cr	38	38	
P(2)[d]	RT → 100	Cr	43 (29−32)	35−36 (∼29)	+13
	140 → 100	is	∼30	∼30	
	70 → RT	LC	34 (∼30)	32−35 (∼30)	
	RT′[d]	LC	36−37, 41	36−41	
P(3)	RT → 100	Cr	68 (41)	34	+13
	140 → 100	is	29	30	
	70 → RT	LC	36	36	
P(4)	RT → 100	Cr	35	35	+20
	140 → 120	is	31	30	
	90	LC	34	34	
	60 → RT	Cr	35	35	
	RT′[e]	LC	37	37	
P(5)	RT → 120	Cr	36	35	+16
	140, 130	is	30	30	
	110	LC	34	34	
	90 → RT	Cr	34	34	

[a] Only Bragg distances determined from the lower angle (not wide angle) XRD reflections are given. The state of the sample is indicated by Cr (crystal), is (isotropic), or LC (liquid crystal). The data for each complex are given in order from ambient temperature (RT) before melting to higher temperatures followed by cooling back to ambient temperature. Values in parentheses indicate additional peaks (the identification of d_1 and d_2 for the Cr phase of **P(3)** is arbitrary). [b] For **P(*X*)**, the length of the small molecule (including van der Waals radius at the tail-end only) is given; in principle, 30 Å should be added to this length for the complexes (length of **P12PP** minus one van der Waals radius plus the hydrogen-bond length). [c] Tendency toward disordered lamellar (smectic A-like) morphology; see ref 29. [d] See text for details. RT′ refers to samples subjected to XRD after variable lengths of time (a few hours to several days) at ambient temperature following cooling from the melt state. [e] Sample cooled from the isotropic state at a rate of 10 °C/min.

30 Å (Table 5). This indicates that the crystallinity observed in the complexes is not a result of phase-separated uncomplexed ***X***.

The isotropic phase (Figure 5b) of all of the complexes gives residual (equidistant) small-angle peaks, which may be a result of short-range (lamellar) order remaining in this phase or may be related to a correlation hole effect.[44,45] These residual peaks are barely visible for **P(1)**, and weak for **P(2)** and **P(3)**, whereas the first-order peak is rather strong for **P(4)** and **P(5)** as also observed for complexes of the same polymer with 4-octylphenol.[10] **P12PP** gives a comparable profile [intermediate between those of **P(2)**/**P(3)** and **P(5)**] at the same temperature (Figure 5b), noting that it is better defined at lower temperatures (Figure 5a,c). **P12PP** was previously concluded to be characterized by a poorly developed smectic A-like morphology with relatively small domain sizes that progressively decrease further with increasing temperature.[29]

X-ray diffractograms of the liquid crystal (LC) phase of the complexes are shown in Figure 5c, obtained on cooling only for all except **P(4)** for which it was obtained on both heating and cooling (including at ambient temperature after cooling from the melt at a rate of 10 °C/min). These diffractograms are all characterized by an amorphous halo at wide angles, indicative of disordered mesophases. For **P(4)** and **P(5)**, there are two sharp reflections at small angles, the first much more intense than the second, like for the partially crystalline phase. Their 1:2 reciprocal spacing is consistent with a lamellar mesophase, as concluded for LC mesophases in other polyamphiphile complexes.[10,19,20] A similar pattern is observed for **P(1)** and **P(3)**, but with somewhat broader and less intense diffraction peaks, indicative of shorter (lamellar) correlation lengths. {These peaks are better defined for **P(3)** after 2 weeks at 70 °C albeit accompanied by a small amount of crystallization [dotted line in Figure 5d; not tested for **P(1)**]}.

For **P(2)**, the diffractogram shown in Figure 5c indicates that what is thought to be a second-order peak is the most intense small-angle peak to develop in the mesophase,[46] whereas the broad and weak lower-angle peak could be a combination of the (weaker) first-order peak and the residual small-angle reflection of the isotropic phase, located at somewhat different angles. However, it was noted that the details of the XRD profile for this complex appeared to be dependent on the sample and thermal history.[41] In particular, there were indications of a memory effect analogous to that observed for semicrystalline polymers; i.e., the thermal and structural characteristics appeared to be influenced by the temperature and time in the melt (that could not be attributed to degradation according to NMR verification). When cooled to ambient at a faster rate (e.g., 10 °C/min) from the isotropic phase, structural order tended to be poorly developed and gave lower Bragg spacings (32−35 Å), suggesting a strong isotropic component, whereas, after a longer time at ambient or after annealing at a higher temperature (e.g., dotted curve in Figure 5d), the order was better defined and gave larger Bragg spacings (36−41 Å). This indicates that there are unusually strong kinetic effects on the formation of the LC phase of **P(2)**. Analysis of the profiles of **P(2)** before melting suggests a similar effect. These effects are reflected in the Bragg spacings given in Table 5 for this complex. In other words, the X-ray profiles of **P(2)** seem to result from a superposition of at least two phases (crystal with liquid crystal and/or isotropic before melting; liquid crystal with isotropic after cooling from the melt). Complex **P(3)**, in contrast, did not show such kinetic effects on the LC phase, but only on the crystalline phase, which is more common.

The Bragg spacings (d_B) derived from the low-angle X-ray reflections are listed in Table 5. For **P(4)** and **P(5)**, where the complexants—especially **4**—have alkyl tails of notable length (and quite different from each other), the Bragg spacings in the LC and crystalline phases are the same as for **P12PP** (36 ± 1 Å at ambient). Furthermore, they are significantly smaller than the total length (l_C) of the polymer side-chain plus small molecule in extended conformation (see Table 5). These observations concord with those for other (ion-exchanged or hydrogen-bonded) pyridinium-based polyamphiphile complexes with small molecules (surfactants) possessing a flexible alkyl chain.[10,19,20] In other words, the Bragg spacing appears to depend only on the host polyamphiphile and its spacer length,[20,29] and not on either the presence or the length of the complexed small molecule.[10,19,20] This suggests that the (flexible) surfactant is accommodated within the same packing structure as the parent polyamphiphile.[10,19,20] **P12PP** and similar polyamphiphiles, given that their Bragg spacings are between one and two (extended) side-chain lengths, were previously concluded to have orthogonal partial bilayer (smectic A) packing.[29]

Possible packing models for this situation, where added small molecules have little effect on the lamellar periodicity and at the same time allow some crystallinity, are discussed in ref 19 (the complexants there being alkyl sulfonates that are ionically complexed to a methylpyridinium moiety). Figure 6 presents similar packing models, adapted to the materials of the present study, for **P12PP** (diagram a) and complexes **P(4)** and **P(5)** (diagram b). The model for **P12PP** is shown with greater

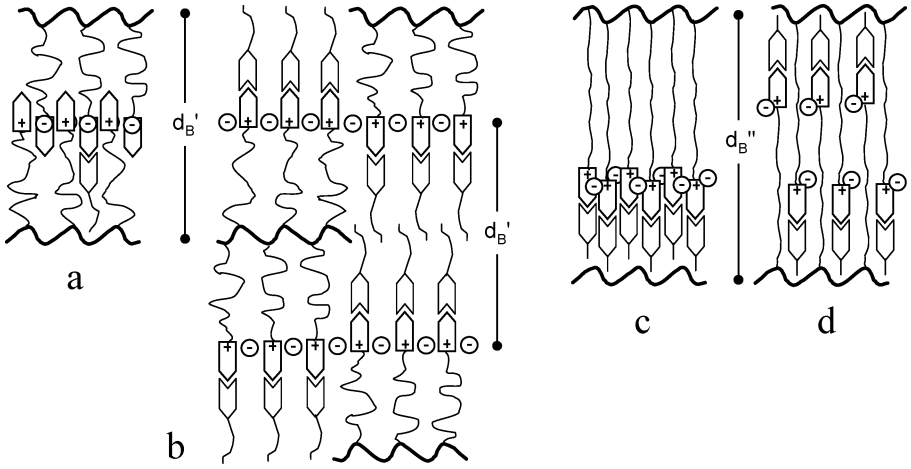

Figure 6. Schematics of possible packing models: (a) for **P12PP** (with a single complexant for illustration purposes); (b) for **P(4)** and **P(5)**; (c) simple single-layer and (d) fully interdigitated bilayer models for **P(1)**, **P(2)**, and **P(3)**. See text for details, and Supporting Information for three-dimensional analogues of models a and b.

interdigitation of the pyridinium moieties than that in refs 19 and 29, giving a single (rather than double) ionic sublayer. This reflects more closely the constancy in Bragg spacing in going from diagram a for **P12PP** to diagram b for the complexes; it also "frees" the pyridyl extremities for H-bonding by the complexant. In diagram b, the key point is the continuity in the ionic subplanes combined with randomly alternating placement of the alkyl spacer on either side of this plane in the form of domains or blocks of variable width. The side chains are shown to be splayed relative to the backbone and fill a lateral molecular area corresponding to roughly twice that of the PP moiety. A "block" of oppositely oriented complexant pairs can then adapt to the remaining space as illustrated, with possible overlap of the alkyl tails permitting potential crystallinity at this level. In this way, the periodicity is governed by twice the spacing between the ionic subplane and the polymer backbone independently of the complexant length.

It may be thought that insertion of the complexant into the packing structure in the manner shown for a single (gray-colored) molecule in Figure 6a, where the mesogenic moieties are all in the same plane, may be more straightforward; however, as discussed in refs 19 and 20, the lamellar thickness would then be expected to increase to accommodate the additional volume and, furthermore, it seems difficult to rationalize crystallization in this arrangement. On the other hand, the Supporting Information illustrates two ways in which complexed side chains may be arranged laterally in two dimensions, one model leading to a variant of Figure 6a, with the oppositely oriented side chains displaced relative to each other, and the other corresponding to Figure 6b. Both arrangements seem plausible (although crystallinity should be more favorable in the second arrangement), and they may be viewed as two limiting cases for a packing structure that may vary from one extreme to the other throughout the material.

By contrast with **P(4)** and **P(5)**, the Bragg spacings for **P(1)** are comparable (within 10%) to the total molecular length of the complex. It is also noteworthy that the d_B of its LC phase at 85 °C is higher than those of **P(4)** and **P(5)** at the similar temperatures of 90 and 110 °C, respectively, despite the fact that **4** and **5** are longer molecules than **1** (Table 5). This suggests that the packing structure of **P(1)** corresponds to a single-layer or effective single-layer (e.g., fully interdigitated bilayer[47]) smectic A phase. This appears to be true for the LC phase of **P(2)** as well, although masked by the complex thermal history effects mentioned earlier, and is more ambiguous for **P(3)**. The crystallized form of **P(2)** and **P(3)** also have significantly higher d_B's. These data may be correlated with the fact that **1**−**3** are all more rigid molecules, with stronger chemical dissimilarities between the complexant and the polymer alkyl spacer. This suggests that the basic packing structure of the parent polyamphiphile is maintained in the complexes only if the small molecule is sufficiently flexible and/or if it has sufficient miscibility with the polyamphiphile spacer (both of these characteristics would be favorable for the stability of the model shown in Figure 6b, in particular considering the two-dimensional lateral side-chain packing illustrated in the Supporting Information). Two possible single-layer packing models are illustrated in Figure 6 (diagrams c and d), where the alkyl spacers are shown to be in more extended form (confined to a lateral molecular area of about one PP moiety) due to closer packing of the mesogenic cores. From the points of view of nanophase separation and optimized ionic interactions, the single-layer model in Figure 6c seems more appropriate than the fully interdigitated bilayer model in Figure 6d.

For comparison, it is of interest to note that the closest nonionic analogues to the present complexes for which XRD data are given (the same polyacrylate-based benzoic acid-terminated comb polymers hydrogen-bonded with stilbene derivatives as mentioned above, but for polymer side-chain spacers of six methylenes only) give Bragg spacings for the smectic A phase that correspond closely to a single complexed side-chain length for complexants with methoxy and hexyloxy tails, but are several Å shorter for complexants with the polar cyano and nitro tails.[42] Clearly, these results are quite different from those for the present ion-containing complexes, indicating that the ionic groups play a primary role in the molecular packing structure, modulated by the nature of the complexant tail.

Finally, it is noted that there is no evidence of a smectic C (or C*) mesophase in any of the complexes, in particular those obtained with the small molecules having chiral tails [**P(4)** and **P(5)**]. This is deduced, in particular, from the fact that the Bragg spacings for the liquid crystal phases of **P(4)** and **P(5)** are about the same as those of similar complexes with flexible tails of variable lengths[10,19,20] (one of which was verified by XRD in oriented state, indicating smectic A order[19]), but also from the fact that the Bragg spacing for the liquid crystal phase of **P(4)** at 90 °C is lower than at ambient (as is typical of SmA phases) whereas the opposite is normally expected for smectic C phases.[40,48] This is consistent with the general observation in

the literature to date that liquid crystalline materials with ionic groups only occasionally give smectic C (and nematic) phases.[4e] In contrast, an analogous hydrogen-bonded complex without the presence of ionic groups does seem to lead to a chiral smectic C phase.[49]

Conclusions

This study of supramolecular liquid crystalline side-chain polymer complexes highlights the interplay among ionic groups, hydrogen-bonding entities, and highly polar mesogens. The complexes are constructed from an amphiphilic polymethacrylate-based comb homopolymer with dodecyl side chains terminated with a pyridylpyridinium group. It is shown, first of all, that the intended hydrogen-bond complexation between the tail-end pyridyl moiety and phenol-functionalized complexants takes place selectively and completely despite the presence of potentially interfering ionic groups and despite strongly polar moieties in some of the complexants. At the same time, both the ionic groups and the strongly polar moieties have an influence on the thermal and structural behavior of the complexes. In general for these complexes, the presence of the ionic groups maintains relatively high glass transition temperatures (above ambient), despite the lengthy side chains. On the other hand, the effective increase in length of the terminal rigid moiety in the side chain that results from the complexation promotes liquid crystalline character as well as the appearance of partial crystallinity.

For the complexes constructed from phenol derivatives having nonpolar tails, recrystallization from the melt occurs relatively easily (as observed previously for the complex of **P12PP** with octyl phenol[10]), with the longer and branched alkyl tail hampering recrystallization to some extent as commonly observed in liquid crystals. Phenol derivatives having polar tails, in contrast, strongly hamper recrystallization, with the cyano tail appearing to suppress it altogether after melt-cooling. The liquid crystal phase in the complexes studied is either monotropic, enantiotropic or, when melt recrystallization is completely suppressed, effectively enantiotropic. Its thermal stability is less for the polar tails compared to the alkyl tails. The phenol derivative with the cyano tail was observed to have an unusually strong retardation effect on the development of the liquid crystal phase. This strong kinetic effect of the cyano tail on the LC phase formation and of the polar tails on recrystallization, as well as the lower stability of the LC phase in the complexes with polar tails, is attributed to the additive effects of electrostatic interactions among the pyridinium groups and among the polar mesogens on the melt viscosity, and possibly also to dipolar interactions between the polar tails and pyridinium bromide groups in the melt. No evidence for smectic C order was found, which adds to other data in the literature indicating that this phase appears difficult to obtain in ion-containing liquid crystal systems.[4e]

The overall structural order of the LC mesophase in the complexes is the same as that of **P12PP**—i.e., smectic A—except that it is better defined (greater correlation lengths). The SmA order in **P12PP** was previously concluded to be of the partial bilayer type.[29] For the phenol derivatives with flexible tails, the characteristic periodicity (Bragg spacing) appears unaffected and shows no dependence on the length of the complexed derivative. This extends previous observations concerning the insensitivity of the periodicity to the presence and length of the complexant in both hydrogen-bonded and ionically bonded complexes, all of which involved simple surfactant-like molecules.[10,19,20] In contrast, the present study indicates that derivatives without a flexible alkyl tail lead to an increase in mesophase periodicity, despite their being shorter molecules than those with the flexible alkyl tail. This periodicity is comparable to the total length of the **P12PP** side chain and the phenol complexant and, therefore, consistent with single-layer smectic A order. This suggests that only complexed molecules with alkyl chains can adapt to the packing structure of the parent polyamphiphile, which may be related to the flexibility of the alkyl chain and/or its miscibility with the polyamphiphile spacer. Possible models, indicating the dominant role of the ionic interactions, were presented and discussed.

It is noteworthy that **P12PP** is a particularly versatile polyamphiphile in that it can be complexed by both hydrogen-bonding molecules and molecules with anionic functions. Thus, it allows not only a comparison between both types of bonding (as well as metal coordination) using the same host, but, even more interestingly, the simultaneous incorporation of ionically bonded and hydrogen-bonded (or metal-coordinated) complexants in close proximity; for example, with two different appropriately functionalized dyes. A single complexant possessing both types of functionalities—that might, moreover, be conceived to be sensitive to an external stimulus—can also be envisaged.

Acknowledgment. The financial support of NSERC Canada is gratefully acknowledged. The authors are members of the multiuniversity Centre for Self-Assembled Chemical Structures/Centre de recherche sur les matériaux auto-assemblés (CSACS/CRMAA) funded by FQRNT Québec.

Supporting Information Available: Figures showing additional FTIR spectra of the complexes **P(*X*)** compared with their components [at ambient before and after melting, at various temperatures for **P(2)**], ambient temperature X-ray diffractograms of ***X***, and possible three-dimensional models related to Figure 6, diagrams a and b. This material is available free of charge via the Internet at http://pubs.acs.org.

References and Notes

(1) Lehn, J.-M. *Supramolecular Chemistry: Concepts and Perspectives*; VCH: Weinheim, Germany, 1995.
(2) Schneider, H.-J.; Yatmirsky, A. *Principles and Methods in Supramolecular Chemistry*; Wiley: Chichester, U.K., 2000.
(3) Lawrence, D. S.; Jiang, T.; Levett, M. *Chem. Rev.* **1995**, *95*, 2229.
(4) See, e.g., the following reviews and references therein: (a) Bazuin, C. G. In *Mechanical and Thermophysical Properties of Polymer Liquid Crystals*; Brostow, W., Ed.; Chapman and Hall: London, 1998; Vol. 3; Chapter 3. (b) Kato, T. *Struct. Bonding (Berlin)* **2000**, *96*, 95. Kato, T. In *Handbook of Liquid Crystals*; Demus, D., Goodby, J. W., Gray, G. W., Speiss, H. W., Vill, V., Eds.; Wiley-VCH: Weinheim, Germany, 1998, Vol. 2B, p 969. (c) Paleos, C. M.; Tsiourvas, D. *Liq. Cryst.* **2001**, *28*, 1127. (d) Masson, P.; Guillon, D. *Mol. Cryst. Liq. Cryst.* **2001**, *362*, 313. (e) Binnemans, K. *Chem. Rev.* **2005**, *105*, 4148. (f) Pollino, J. M.; Weck, M. *Chem. Soc. Rev.* **2005**, *34*, 193. (g) Kato, T.; Mizoshita, N.; Kishimoto, K. *Angew. Chem., Int. Ed.* **2006**, *45*, 38.
(5) Lu, X.; He, C.; Griffin, A. C. *Macromolecules* **2003**, *36*, 5195.
(6) Medvedev, A. V.; Barmatov, E. B.; Medvedev, A. S.; Shibaev, V. P.; Ivanov, S. A.; Kozlovsky, M.; Stumpe, J. *Macromolecules* **2005**, *38*, 2223.
(7) Cui, L.; Zhao, Y. *Chem. Mater.* **2004**, *16*, 2076. Cui, L.; Dahmane, S.; Tong, X.; Zhu, L.; Zhao, Y. *Macromolecules* **2005**, *38*, 2076.
(8) Huang, W.; Han, C. D. *Macromolecules* **2006**, *39*, 4735.
(9) Xu, H.; Hong, R.; Lu, T.; Uzun, O.; Rotello, V. M. *J. Am. Chem. Soc.* **2006**, *128*, 3162.
(10) Bazuin, C. G.; Brodin, C. *Macromolecules* **2004**, *37*, 9366.
(11) Valkama, S.; Ruotsalainen, T.; Nykänen, A.; Laiho, A.; Kosonen, H.; ten Brinke, G.; Ikkala, O.; Ruokolainen, J. *Macromolecules* **2006**, *39*, 9327. Ruokolainen, J.; Mäkinen, R.; Torkkeli, M.; Mäkelä, T.; Serimaa, R.; ten Brinke, G.; Ikkala, O. *Science* **1998**, *280*, 557. Ruotsalainen, T.; Torkkeli, M.; Serimaa, R.; Mäkelä, T.; Mäki-Ontto, R.; Ruokolainen, J.; ten Brinke, G.; Ikkala, O. *Macromolecules* **2003**, *36*, 9437.

(12) This group applied the same concept to polyaniline, to which hexylresorcinol was H-bonded through camphor sulfonic acid, yielding an electrically conducting, cylindrically organized material: Kosonen, H.; Ruokolainen, J.; Knaapila, M.; Torkkeli, M.; Jokela, K.; Serimaa, R.; ten Brinke, G.; Bras, W.; Monkman, A. P.; Ikkala, O. *Macromolecules* **2000**, *33*, 8671 and Kosonen, H.; Valkama, S.; Ruokolainen, J.; Knaapila, M.; Torkkeli, M.; Serimaa, R.; Monkman, A. P.; ten Brinke, G.; Ikkala, O. *Synth. Met.* **2003**, *137*, 881. See also: Ikkala, O.; Knaapila, M.; Ruokolainen, J.; Torkkeli, M.; Serimaa, R.; Jokela, K.; Horsburgh, L.; Monkman, A.; ten Brinke, G. *Adv. Mater.* **1999**, *11*, 1206 and Knaapila, M.; Stepanyan, R.; Horsburgh, L. E.; Monkman, A. P.; Serimaa, R.; Ikkala, O.; Subbotin, A.; Torkkeli, M.; ten Brinke, G. *J. Phys. Chem. B* **2003**, *107*, 14199.
(13) Nair, K. P.; Weck, M. *Macromolecules* **2007**, *40*, 211.
(14) Nair, K. P.; Pollino, J. M.; Weck, M. *Macromolecules* **2006**, *39*, 931. Pollino, J. M.; Stubbs, L. P.; Weck, M. *J. Am. Chem. Soc.* **2004**, *126*, 563.
(15) Hartikainen, J.; Lahtinen, M.; Torkkeli, M.; Serimaa, R.; Valkonen, J.; Rissanen, K.; Ikkala, O. *Macromolecules* **2001**, *34*, 7789. The concept of coordination and ionic bonding combined at a single site, as postulated in this paper, was applied profitably in another system to produce a supramolecular "multicomb" P4VP polymer having several alkyl side chains per repeat unit: Valkama, S.; Lehtonen, O.; Lappalainen, K.; Kosonen, H.; Castro, P.; Repo, T.; Torkkeli, M.; Serimaa, R.; ten Brinke, G.; Leskelä, M.; Ikkala, O. *Macromol. Rapid Commun.* **2003**, *24*, 556.
(16) See, e.g., the following reviews and references therein: (a) Ikeda, T.; Mamiya, J.; Yu, Y. *Angew. Chem., Int. Ed.* **2007**, *46*, 506. (b) Yesodha, S. K.; Pillai, C. K. S.; Tsutsumi, N. *Prog. Polym. Sci.* **2004**, *29*, 45. (c) Kajzar, F.; Lee, K.-S.; Jen, A. K.-Y. *Adv. Polym. Sci.* **2003**, *161*, 1. (d) Ikeda, T. *J. Mater. Chem.* **2003**, *13*, 2037. (e) Natansohn, A.; Rochon, P. *Chem. Rev.* **2002**, *102*, 4139.
(17) Term used to signify molecules possessing a thermotropic mesogenic moiety coupled to a surfactant-like moiety. See, e.g., ref 38.
(18) See, e.g., Tork, A.; Bazuin, C. G. *Macromolecules* **2001**, *34*, 7699.
(19) Vuillaume, P. Y.; Bazuin, C. G. *Macromolecules* **2003**, *36*, 6378.
(20) Vuillaume, P. Y.; Sallenave, X.; Bazuin, C. G. *Macromolecules* **2006**, *39*, 8339.
(21) Bernhardt, H.; Weissflog, W.; Kresse, H. *Liq. Cryst.* **1998**, *24*, 895. Sahin, Y. M.; Diele, S.; Kresse, H. *Liq. Cryst.* **1998**, *25*, 175. Kresse, H. *Liq. Cryst.* **1998**, *25*, 437.
(22) Tsiourvas, D.; Paleos, C. M.; Skoulios, A. *Liq. Cryst.* **1999**, *26*, 953.
(23) Hao, X.; Heuts, J. P. A.; Barner-Kowollik, C.; Davis, T. P.; Evans, E. *J. Polym. Sci., Part A: Polym. Chem.* **2003**, *41*, 2949. Nakano, T.; Hasegawa, T.; Okamoto, Y. *Macromolecules* **1993**, *26*, 5494. Allcock, H. R.; Kim, C. *Macromolecules* **1990**, *23*, 3881. Duran, R.; Gramain, P. *Makromol. Chem.* **1987**, *188*, 2001.
(24) Jones, B. A.; Bradshaw, J. S.; Nishioka, M.; Lee, M. L. *J. Org. Chem.* **1984**, *49*, 4947.
(25) Ringsdorf, H.; Schmidt, H. W. *Makromol. Chem.* **1984**, *185*, 1327. Rozes, L.; Noël, C.; Campistron, I.; Thomas, M.; Reyx, D.; Kajzer, F. *Macromol. Chem. Phys.* **1998**, *199*, 2553. Aubertin, F.; Zhao, Y. *J. Polym. Sci., Part A: Polym. Chem.* **2004**, *42*, 3445.
(26) Cui, Y.; Qian, G.; Gao, J.; Chen, L.; Wang, Z.; Wang, M. *J. Phys. Chem. B* **2005**, *109*, 23295. Liu, J.-H.; Yang, P.-C. *J. Appl. Polym. Sci.* **2004**, *91*, 3693. Wu, X.; Zhang, G.; Zhang, H. *Macromol. Chem. Phys.* **1998**, *199*, 2101. Wu, L.; Tuo, X.; Cheng, H.; Chen, Z.; Wang, X. *Macromolecules* **2001**, *34*, 8005.
(27) Tian, Y.; Xie, J.; Wang, C.; Zhao, Y.; Fei, H. *Polymer* **1999**, *40*, 3835. Zheng, Z.; Xu, J.; Sun, Y.; Zhou, J.; Chen, B.; Wang, K. *J. Polym. Sci., Part A: Polym. Chem.* **2006**, *44*, 3210.
(28) Brodin, C. Ph.D. Thesis, Dép. de chimie, Université Laval, Québec, 2003.
(29) Vuillaume, P. Y.; Bazuin, C. G.; Galin, J. C. *Macromolecules* **2000**, *33*, 781.
(30) This molecular weight is consistent with the T_g measured, with reference to a T_g vs molecular weight curve determined in ref 28.
(31) For the small molecules, the position of maximum absorption varies: it is located near 3400 cm^{-1} for **1**, **3**, and **5** and 3300 cm^{-1} for **2**, with **1** showing a second (slightly less intense) maximum near 3370 cm^{-1}. In comparison, octylphenol was previously shown to give two maxima at 3400 and 3360 cm^{-1}, which were attributed to adsorbed water and the hydroxyl stretch of hydrogen-bonded self-associated phenol groups, respectively.[10] However, the small molecules in the present study appear not to contain water according to elemental analysis (see Experimental Section), and also according to the thermogravimetric analysis of a sample not subjected to prior in situ treatment at 100 °C. This suggests that the maximum near 3400 cm^{-1} is not related to adsorbed water, but rather to the hydroxyl stretch in the self-associated molecules. Its position (reflecting also the hydrogen bond strength) may be influenced by resonance effects of the (azo)phenyl substituents as well as by the crystal structure adopted.
(32) Isasi, J. R.; Cesteros, L. C.; Katime, I. *Macromolecules* **1994**, *27*, 2200.
(33) Moskala, E. J.; Varnell, D. F.; Coleman, M. M. *Polymer* **1985**, *26*, 228.
(34) Ruokolainen, J.; Torkkeli, M.; Serimaa, R.; Vahvaselkä, S.; Saariaho, M.; ten Brinke, G.; Ikkala, O. *Macromolecules* **1996**, *29*, 6621.
(35) Data obtained by C. Brodin in the laboratory of C. G. Bazuin.
(36) The transition temperatures for **1**−**3** may be affected by slight degradation, given that the 2% weight loss temperature according to TGA (which may reflect vaporization as well as degradation) occurs below the melting point for these compounds. Subsequent DSC scans for **3** indeed gave a lower melting point (see Table 1)—not verified for **1** and **2**—whereas **4** and **5** gave identical values in subsequent scans.
(37) Cowie, J. M. G.; Haq, Z.; McEwen, I. J.; Velickovic, J. *Polymer* **1981**, *22*, 327. Cowie, J. M. G.; McEwen, I. J.; Pedram, M. Y. *Macromolecules* **1983**, *16*, 1151. Arrighi, V.; Triolo, A.; McEwen, I. J.; Holmes, P.; Triolo, R.; Amenitsch, H. *Macromolecules* **2000**, *33*, 4989. Arrighi, V.; McEwen, I. J.; Holmes, P. F. *Macromolecules* **2004**, *37*, 6210. Hahn, B.; Percec, V. *Macromolecules* **1987**, *20*, 2961. Percec. V.; Hahn, B. *Macromolecules* **1989**, *22*, 1588. Percec. V.; Hahn, B.; Ebert, M.; Wendorff, J. H. *Macromolecules* **1990**, *23*, 2095. Emmerling, U.; Lindau, J.; Diele, S.; Werner, J.; Kresse, H. *Liq. Cryst.* **2000**, *27*, 1069. Hiller, S.; Pascui, O.; Budde, H.; Kabisch, O.; Reichert, D.; Beiner, M. *New J. Phys.* **2004**, *6*, 10. Beiner, M.; Huth, H. *Nat. Mater.* **2003**, *2*, 595.
(38) Tibirna, C. M.; Bazuin, C. G. *J. Polym. Sci., Part B: Polym. Phys.* **2005**, *43*, 3421.
(39) It confirms what was reported in ref 28 for this complex.
(40) Collings, P. J.; Hird, M. *Introduction to Liquid Crystals, Chemistry and Physics*; Taylor & Francis: London, 1997.
(41) Furthermore, aging of **P(2)** in closed vials at ambient temperature, contrary to the other complexes, appeared to reduce the amount of crystallinity, as indicated by both DSC and XRD. Possibly, this is related to gradual absorption of H_2O.
(42) Kato, T.; Kihara, H.; Ujiie, S.; Uryu, T.; Fréchet, J. M. J. *Macromolecules* **1996**, *29*, 8734.
(43) McArdle, C. B., Ed. *Side Chain Liquid Crystal Polymers*; New York: Chapman and Hall, 1989.
(44) Lipatov, Y. S.; Shilov, V. V.; Tsukruk, V. V. *Macromolecules* **1986**, *19*, 1308.
(45) Ruokolainen, J.; Torkkeli, M.; Serimaa, R.; Komanschek, B. E.; Ikkala, O.; ten Brinke, G. *Phys. Rev. E* **1996**, *54*, 6646. Huh, J.; Ikkala, O.; ten Brinke, G. *Macromolecules* **1997**, *30*, 1828.
(46) Unusually intense second-order peaks in LC phases are generally attributed to an additional plane of higher electron density within the layers. See, for example: Davidson, P. *Prog. Polym. Sci.* **1996**, *21*, 893.
(47) Barón, M. *Pure Appl. Chem.* **2001**, *73*, 845.
(48) Heinrich, B.; Guillon, D. *Mol. Cryst. Liq. Cryst.* **1995**, *268*, 21.
(49) Kumar, U.; Fréchet, J. M. J.; Kato, T.; Ujiie, S.; Timura, K. *Angew. Chem., Int. Ed. Engl.* **1992**, *31*, 1531.

MA070689T